

## Full length article

# In situ observation of magnetic vortex manipulation by external fields in amorphous CeFeB ribbon



Shulan Zuo <sup>a,b</sup>, Ming Zhang <sup>a</sup>, Rui Li <sup>a,b</sup>, Ying Zhang <sup>a,\*</sup>, Licong Peng <sup>a,b</sup>, Jiefu Xiong <sup>a,b</sup>, Dan Liu <sup>a,b</sup>, Tongyun Zhao <sup>a</sup>, Fengxia Hu <sup>a,b</sup>, Baogen Shen <sup>a,b,\*</sup>, Jirong Sun <sup>a,b</sup>

<sup>a</sup> State Key Laboratory of Magnetism, Institute of Physics, Chinese Academy of Sciences, Beijing 100190, PR China

<sup>b</sup> University of Chinese Academy of Sciences, Beijing, 100049, PR China

## ARTICLE INFO

## Article history:

Received 9 May 2017

Received in revised form

25 June 2017

Accepted 27 July 2017

Available online 28 July 2017

## ABSTRACT

In this study, we show the real-space observation of the magnetic domain configuration in amorphous Ce<sub>14</sub>Fe<sub>80</sub>B<sub>6</sub> ribbon using Lorentz transmission electron microscopy. Cross-tie domain walls composed of magnetic vortices (Vs) and antivortices (AVs) are observed. The evolution of Vs/AVs manipulated by temperature, in-plane magnetic field, and electrical current is clearly demonstrated. Magnetic V nucleation and annihilation in pair are observed because of the stimulus of external fields.

© 2017 Acta Materialia Inc. Published by Elsevier Ltd. All rights reserved.

## Keywords:

Magnetic domain

Nucleation

Amorphous

External field manipulation

Lorentz microscopy

## 1. Introduction

The manipulation of noncollinear or noncoplanar spin textures, such as magnetic domain wall (DW) propagation in racetrack memory, vortex (V) and skyrmion dynamic behavior, has attracted significant research interest because of the underlying fundamental science and technical applications [1–6]. The spatial region for one conventional magnetic bit is reaching its fundamental limit, thereby restricting improvements in the storage capacity of the magnetic disk. A number of alternatives to overcome this limit have been suggested. Racetrack memory with digital data stored in a series of movable magnetic DWs was first demonstrated in a magnetically soft permalloy nanowires [7]. When electric current traverses a magnetic DW, spin angular momentum is transferred from electrons to spins, leading to DW propagation [8]. The particle-like magnetic skyrmion, nontrivial bubble, and V with a size of 10–100 nm are appealing as basic units because of their topological properties and efficient current-driven behavior, thereby presenting potential applications for high-density

information-bit data storage and spintronic devices [1].

Uniaxial magnetic anisotropy is an important parameter that determines the topological spin configuration. Skyrmions are usually obtained with medium anisotropy, whereas magnetic bubbles are formed with strong anisotropy. V is favored when the anisotropy is very weak and the in-plane magnetization is dominant [9]. The Chern number or winding number  $w$  is commonly used to identify the topology. The magnetization distributions of V and antivortex (AV) are related via the winding number  $w = -1$  for AV and  $w = +1$  for V [10]. The total winding number of the thin-film element is a topological invariant that consists of V/AV pairs. The V state with perpendicular magnetization at the core site [10–12] is a stable magnetic configuration for soft ferromagnetic platelet DWs. Circular configuration with a curling in-plane magnetic configuration (V) and the related spin-transfer torque-driven DW behavior can be considered distinct elements for magnetoelectronic random access memory [1]. While experimental control behavior of DWs has been observed, the underlying physical mechanisms between electric current and magnetization have yet to be clarified [8,13–17].

Significant experiments and theories have been devoted to understand the dynamics of Vs and the magnetization reversal behavior. The gyroscopic motion of the V core was observed by micromagnetic simulations and experiments [2,18–21]. The

\* Corresponding authors. State Key Laboratory of Magnetism, Institute of Physics, Chinese Academy of Sciences, Beijing 100190, PR China.

E-mail addresses: [zhangy@iphy.ac.cn](mailto:zhangy@iphy.ac.cn) (Y. Zhang), [shenbg@iphy.ac.cn](mailto:shenbg@iphy.ac.cn) (B. Shen).

temperature dependency and the magnetization reversal behavior based on V nucleation/annihilation [20,21] along the cross-tie wall have been investigated in patterned films [3,13,14,22,23], where edge constriction introduces special spin orientation. Theoretical prediction and experimental results show that V/AV core periodically nucleates in pair [24,25]. The density and dynamics manipulation of magnetic Vs are important for the potential application as magnetic-memory units. However, most studies were performed via magnetic property measurements without direct in-situ observation, and the experimentally dynamic behavior was mostly limited to permalloy sample with constraint shapes. CeFeB alloys were previously studied as permanent nanocrystalline magnets [26–28], as well as amorphous magnetic refrigerant material [29]. The overconsumption of Nd and Pr elements [30] for permanent magnets resulted in intense demand for balanced use of the rare-earth resource. Thus, exploring the magnetic domain structures, in-situ magnetization reversal behavior, and phase transition behavior in novel magnets with low-cost but surplus rare-earth elements, such as Ce and La, would be of great interest. Our findings about magnetic V evolution in amorphous Ce<sub>14</sub>Fe<sub>80</sub>B<sub>6</sub> without pattern constriction will provide a fruitful playground for the exploration of fundamental physics and will open the door to take advantage of diversified rare-earth resources.

## 2. Experimental

Polycrystalline Ce<sub>14</sub>Fe<sub>80</sub>B<sub>6</sub> ingot is synthesized by using arc melting technique in a high-purity argon atmosphere, and amorphous ribbons are prepared by using single-roller melt spinning method. The details of the preparation and other magnetic performances will be reported elsewhere. Two Lorentz transmission electron microscopy (LTEM) samples are cut from a piece of ribbon and thinned via focused-ion-beam (FIB) method and conventional ion milling method, respectively. To image the crystal microstructure and magnetic domain configuration, a JEOL-dedicated LTEM is used with almost no magnetic remnant field around the sample. In situ TEM observations of magnetic domain evolution under external fields are conducted using a liquid-nitrogen TEM sample holder (100–300 K), an in-plane magnetization holder, and an electric current holder. With the use of the Fresnel LTEM method, the magnetic DWs can be imaged as converges (bright contrast) or diverges (dark contrast) of the electron beam on the defocused (under or overfocused) image planes by the Lorentz force. The high-resolution in-plane magnetization distribution map is obtained using the commercial QPt software based on the transport of the intensity equation (TIE) with three sets of images with under, over, and in (or zero) focal lengths. The colors depict the magnitude and direction of the lateral magnetizations, which can be deduced from the arrows and the color wheel.

## 3. Results and discussion

### 3.1. Temperature dependence of cross-tie domain wall configuration

The temperature dependence of the magnetic domain evolution of the TEM sample prepared via conventional ion-milling method is shown in Fig. 1. The amorphous structure is confirmed by selected area electron diffraction, as shown in the inset of Fig. 1a. The in-situ cooling experiments from 293 to 125 K (Fig. 1a–e) and the heating experiments from 125 to 293 K (Fig. 1f–h) demonstrate the appearance of cross-tie DW and the augmentation of V/AV at low temperature. The V nucleation and annihilation agree well with the preceding report [31], demonstrating that V persists longer with decreased thermal activation at low temperatures. Meanwhile, the decrease in saturation magnetization facilitates V annihilation at

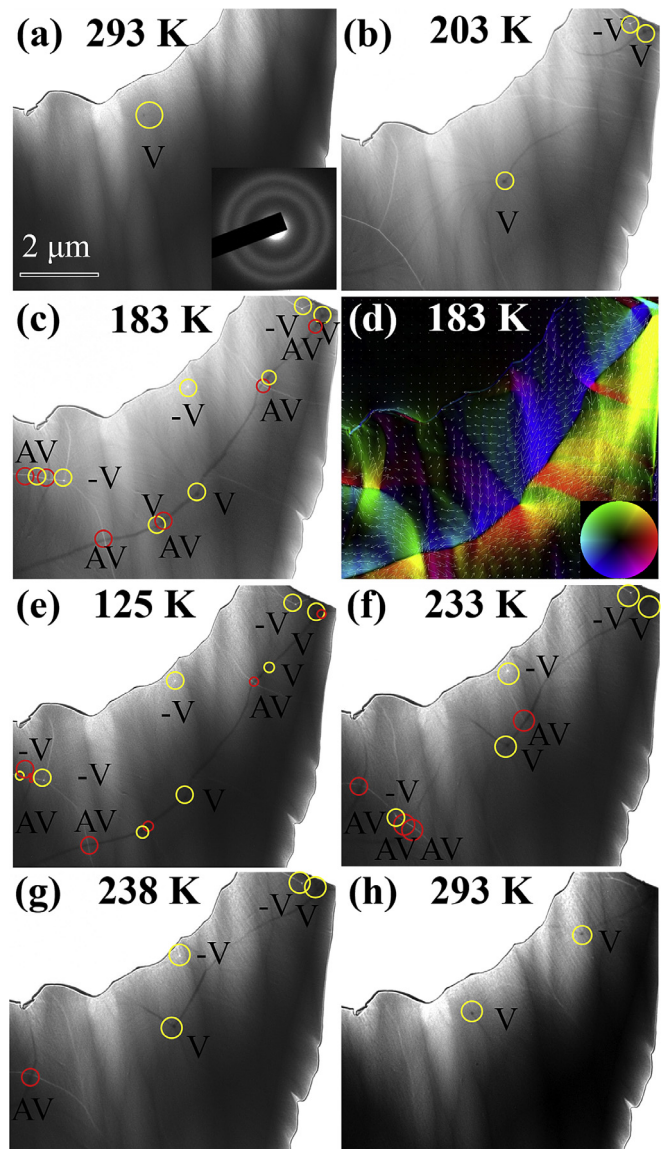


**Fig. 1.** LTEM images for temperature dependence of magnetic vortices (Vs) in amorphous Ce<sub>14</sub>Fe<sub>80</sub>B<sub>6</sub> sample prepared via ion milling. The underfocused LTEM image of magnetic domain evolution from individual vortex (V) at (a) 293 K, domain walls at (b) 203 K to cross-tie wall with increasing V/AV pairs at (c) 183 K and (e) 125 K is shown. The inset of (a) is the selected area electron diffraction with amorphous characteristic of the ribbon. (d) Corresponding in-plane magnetic texture of (c) obtained by TIE analysis with the magnitude and orientation of the magnetization depicted by the color and the arrows. (f)–(h) The magnetic domain evolution when increasing the temperature with broken cross-tie wall and decreased V/AV pairs. The cores of magnetic V/AV are marked in red for AVs and yellow for Vs, and the opposite chirality of V is depicted as V and -V with dark and bright contrast. (For interpretation of the references to colour in this figure legend, the reader is referred to the web version of this article).

high temperature.

The Curie temperature is approximately 270 K as seen in  $M-T$  curve (Fig. 2a). However, the  $1/\chi-T$  (inversion of susceptibility versus temperature) displays a notable deviation from the Curie–Weiss law at approximately room temperature (RT). This deviation might be caused by short-range magnetic clusters within a disordered matrix [32–35], which explains the Vs observed at 293 K. Fig. 2b summarizes the temperature dependence of V/AV number based on the LTEM images in Fig. 1. The number (density) of the V/AV increases with decreasing temperature, and stabilized

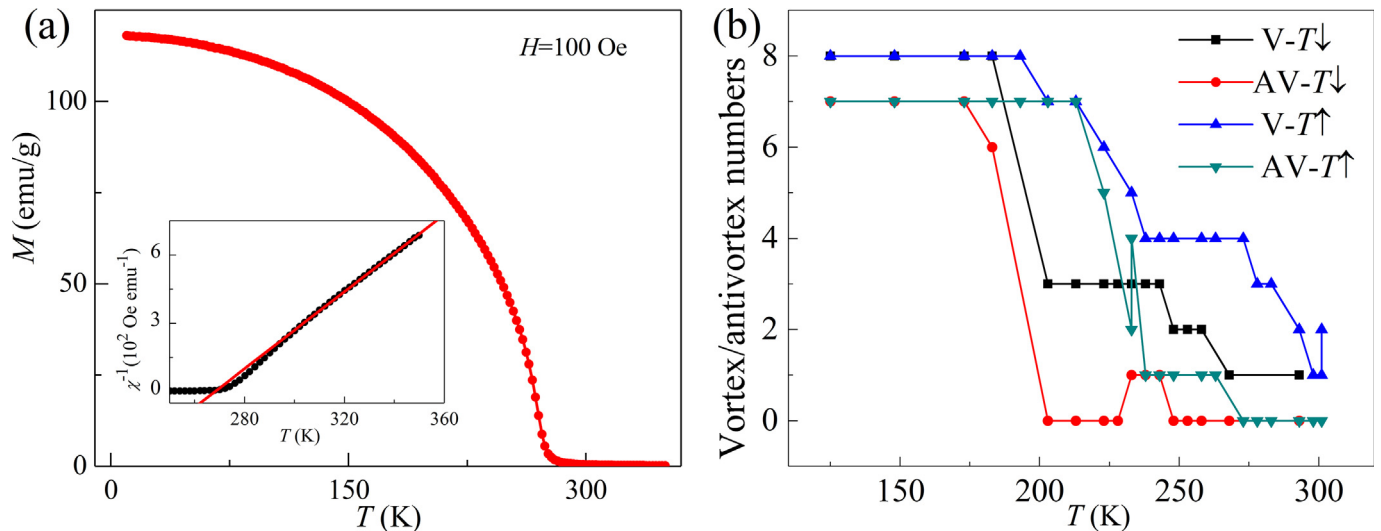


**Fig. 2.** Temperature dependence of magnetic properties in amorphous  $\text{Ce}_{14}\text{Fe}_{80}\text{B}_6$ . (a) Magnetization ( $M$ - $T$ ) curve with temperature. Inset shows the  $1/\chi$ - $T$  (inversion of susceptibility versus temperature) and the Curie-Weiss fitting (red line). (b) The V/AV numbers change with temperature based on LTEM images of conventional ion-milling TEM sample. (For interpretation of the references to colour in this figure legend, the reader is referred to the web version of this article).

Vs/AVs are obtained below a critical temperature. Temperature hysteresis for V/AV number change exists between decreasing and increasing temperature. The curve for V/AV number change is nonlinear with plateau in a certain temperature range, which may indicate the energy barrier for V nucleation/annihilation [31].

The underfocused LTEM image shows in-plane spontaneous V, AV, and tree-like DWs at 293 K (Fig. 3a) for the sample prepared by FIB. The cross-tie DWs that connect V/AV are clearly observed at 278 K as shown in Fig. 3b, replacing tree-like DWs. The red-selected area without obvious defects (Fig. 3b) is selected to study the V/AV evolution connected with cross-tie DW. The underfocused LTEM images demonstrate the temperature dependence of the magnetic textures, as shown in Fig. 3c–f. The inset of Fig. 3c shows the in-

plane magnetic configuration of the cross-tie wall, reconstructed by TIE analysis. Upon cooling from 293 to 123 K, the number of magnetic Vs is increased because of the pairwise nucleation of V and AV similar to the phenomena discussed in Fig. 1 for the TEM sample prepared via ion milling. The thermal fluctuation helps overcome restraining forces, and the DW can statistically hop into a different minimum state [36]. Temperature differences exist between the two TEM samples prepared via different methods. The cross-tie DW with V/AV pairs is observed at 293 K in the sample prepared via FIB process in Fig. 3a, which is probably due to the thin thickness and stress-induced anisotropy change [37,38]. Moreover, the intrinsic magnetic domain configuration obtained via altering the sample thickness was confirmed by micromagnetic simulation,

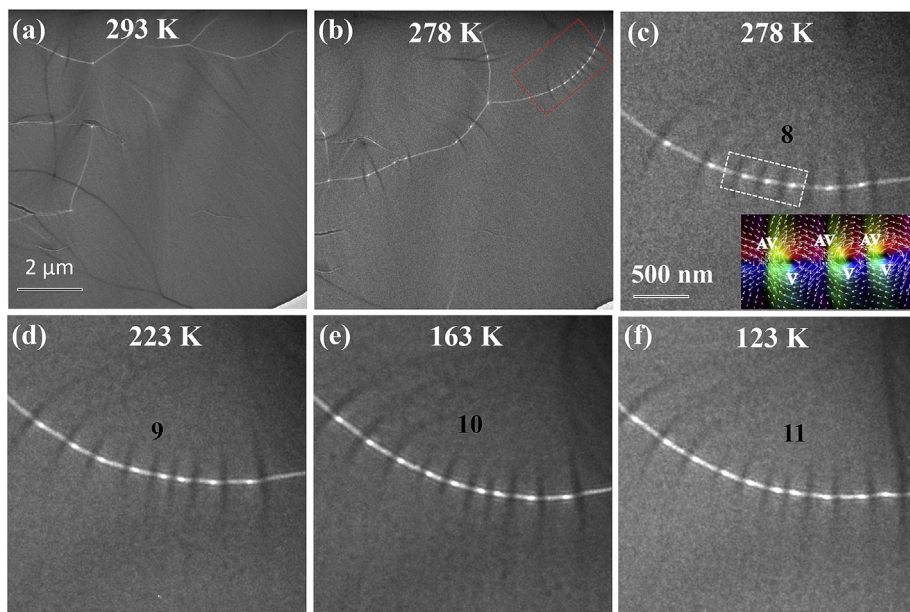


**Fig. 3.** LTEM images for temperature dependence of cross-tie domain wall evolution in amorphous  $\text{Ce}_{14}\text{Fe}_{80}\text{B}_6$  ribbon prepared by FIB. The overall LTEM image of the magnetic domain by in situ cooling from (a) 293 K to (b) 278 K is shown. The enlarged cross-tie domain wall for the selected area with increased V/AV pairs while decreasing the temperature to (d) 223, (e) 163, and (f) 123 K is presented. The inset of (c) shows the corresponding spin texture of cross-tie wall for the selected area obtained by TIE analysis. The AV numbers are marked out.

as shown in Fig. 7. This finding corresponds well with the isolated Vs in the thick conventional TEM sample and the cross-tie domain in the thin FIB sample.

### 3.2. Magnetic domain evolution under electric current

The magnetic structure with cross-tie DW is scrutinized before switching on the current (Fig. 4a). The magnetization configuration is in situ imaged with the increments of the electric current. V/AV propagation and nucleation/annihilation are observed under electric current excitation by LTEM. An individual V (marked by a yellow rectangle in Fig. 4a) moves toward the edge and disappears

(Fig. 4b) with increasing current. The cross-tie wall is straightened (indicated by red arrows in Fig. 4b) because of the spin torque effect with high electric current, where AVs are enclosed by two adjacent Vs with the same sense of rotation. The cross-tie magnetic domain remains unchanged until pair nucleation of the V and AV is initiated (Fig. 4c) above a critical electric current. As the current increases to 364 mA (Fig. 4d), the V/AV begins to annihilate, in which the V/AV would preferentially disappear if it nucleates later, and vice versa. Temporal relaxation affects the equilibrium position of the V/AV cores, and nucleation/annihilation persists at the same current by rotating the in-plane magnetization ripple. The contrast of both magnetization ripple and V changes greatly in a certain electric

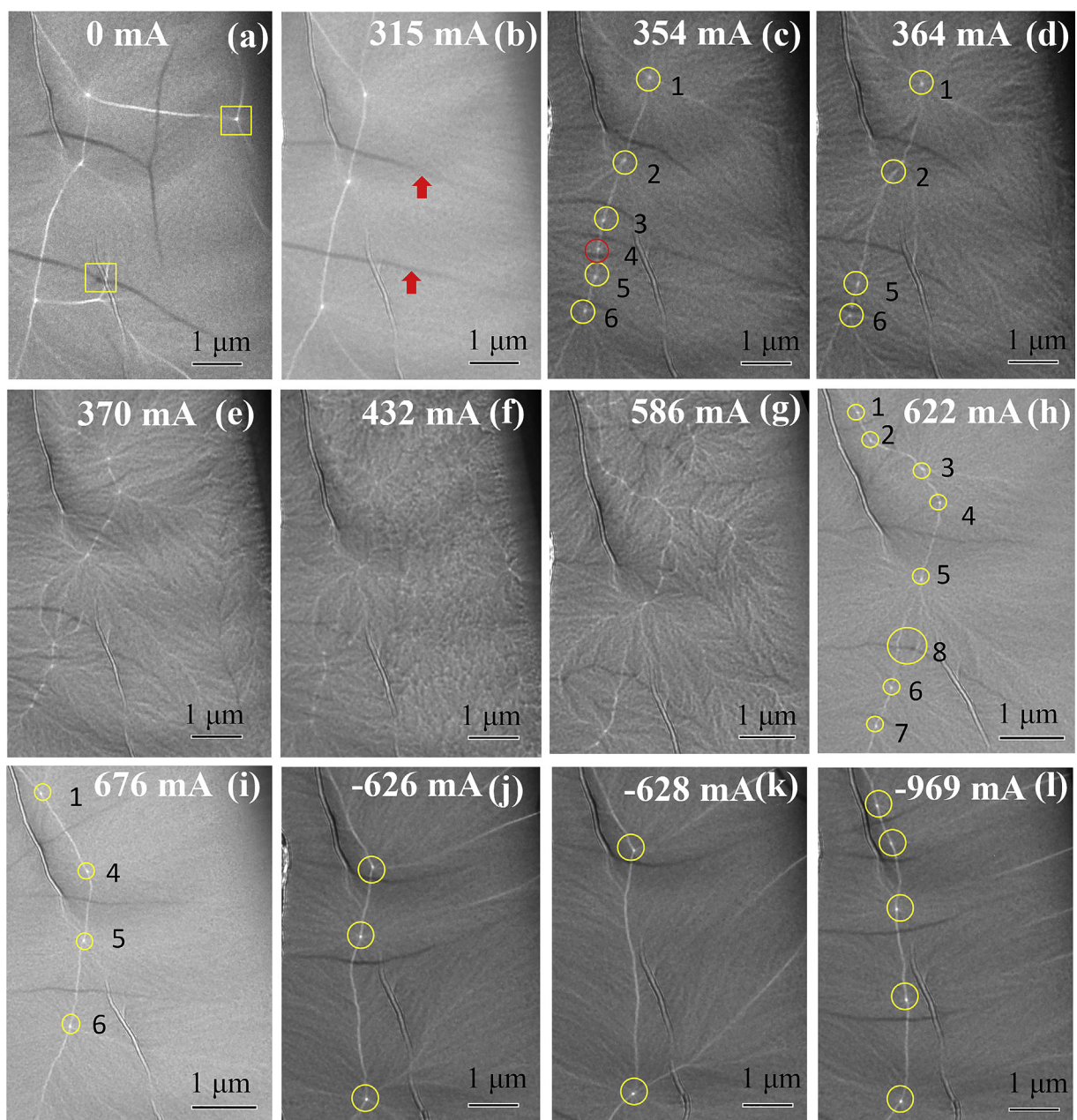


**Fig. 4.** LTEM images for electric current dependence of cross-tie domain wall evolution in amorphous  $\text{Ce}_{14}\text{Fe}_{80}\text{B}_6$  ribbon prepared by FIB. The underfocused LTEM images for nucleation/annihilation and propagation of magnetic domains including V/AV, cross-tie domain walls, and in-plane ripples under electric currents (a) 0, (b) 315, (c) 354, (d) 364, (e) 370, (f) 432, (g) 586, (h) 622, and (i) 676 mA and reversed electric currents (j)  $-626$ , (k)  $-628$ , and (l)  $-969$  mA are shown. The number of vortex cores is marked out. The red and yellow circles denote new and previous cores, respectively. The red arrows indicate straightened cross-tie walls. (For interpretation of the references to colour in this figure legend, the reader is referred to the web version of this article).

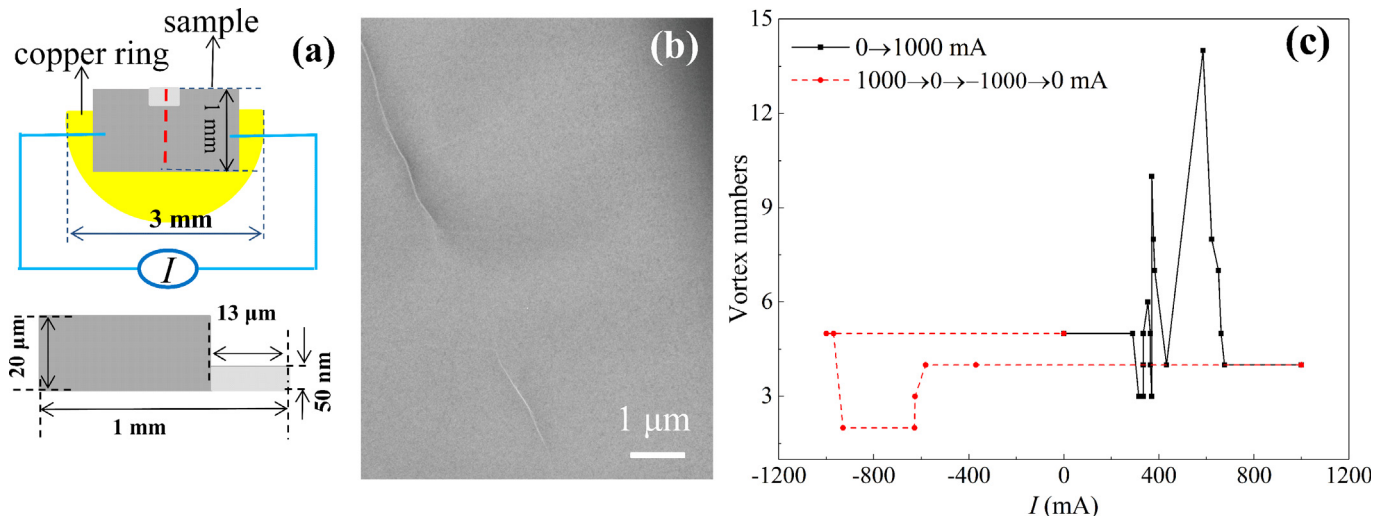


**Fig. 5.** (a) Schematically electric-current manipulation device presenting the plane and cross-section views of FIB TEM sample. (b) The in-focus TEM image of the viewed regions. (c) The summarized numbers of vortex cores versus current ( $I$ ) with the black line for increasing current ( $0 \rightarrow 1000$  mA) in one direction and red dots for decreasing current ( $1000$  mA  $\rightarrow 0$  mA) and the current applied in the reverse direction ( $0$  mA  $\rightarrow -1000$  mA  $\rightarrow 0$  mA). (For interpretation of the references to colour in this figure legend, the reader is referred to the web version of this article).

current range (Fig. 4e and f), indicating the magnetic moment rotational process [39]. The Vs almost totally annihilate (Fig. 4f) at the electric current of 432 mA. The V and AV nucleate again when

the current increases to 574 mA, and annihilate with further increasing current (Fig. 4g and h). Finally, the magnetization configuration is stabilized at cross-tie DW (Fig. 4i) and remains

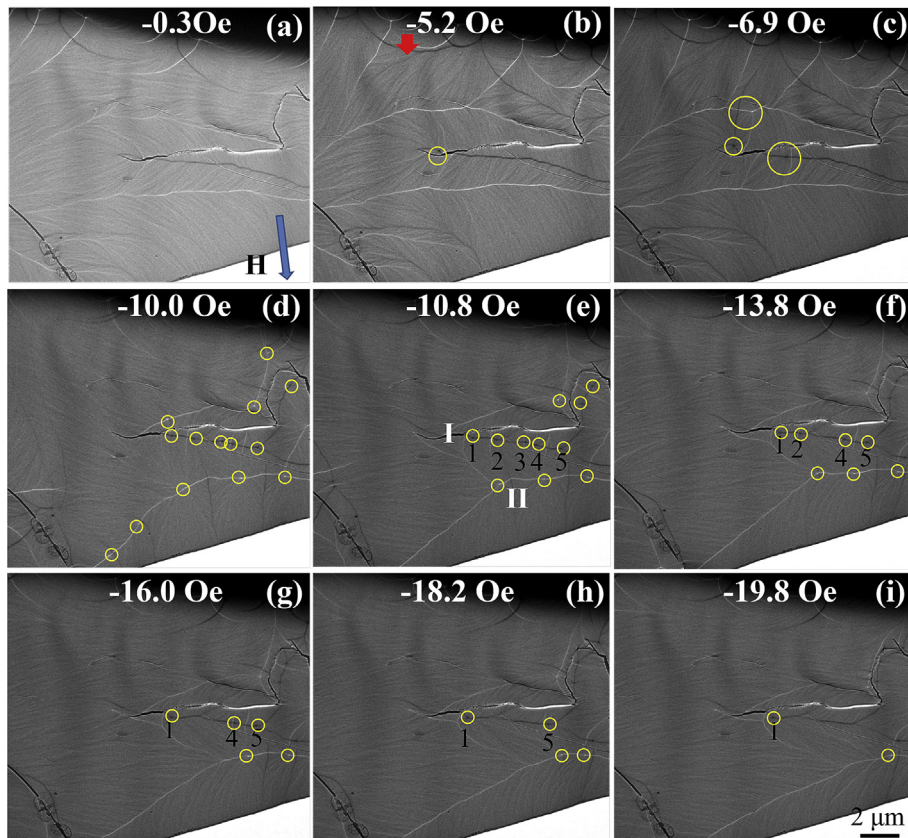


**Fig. 6.** LTEM images of magnetization reversal evolution in amorphous Ce<sub>14</sub>Fe<sub>80</sub>B<sub>6</sub> ribbons prepared by FIB. The underfocused LTEM images for the nucleation/annihilation and propagation of magnetic domains including V/AV, cross-tie domain walls, and in-plane ripples under reversed magnetic field of (a) 0.3, (b) 5.2, (c) 6.9, (d) 10, (e) 10.8, (f) 13.8, (g) 16.0, (h) 18.2, and (i) 19.8 Oe are shown. The blue arrow depicts the direction of the reversed magnetic field. The I, II, and numbers mark the serial number of the main domain walls and vortex in main wall I. The yellow circles present vortex cores. (For interpretation of the references to colour in this figure legend, the reader is referred to the web version of this article.)

unchanged even when the current is further increased to 1000 mA and reduced to zero (not shown). The V and AV annihilate under a reversed electric current (Fig. 4j and k) and then renucleate (Fig. 4l) as the reversed current increases above a critical value. The magnetic structure at a current of −969 mA (Fig. 4l) is stabilized even after the electric current is switched off.

The above electric current manipulation is conducted on the Ce<sub>14</sub>Fe<sub>80</sub>B<sub>6</sub> TEM sample fabricated via FIB, which is schematically shown in Fig. 5a with the plane and cross-section views of current-driven microdevice. A bright field TEM image (in focus) of this region is shown in Fig. 5b with uniform diffraction contrast except two line defects. The FIB TEM sample is used for electric current manipulation due to the uniform thickness and electric current distribution. The summarized representative curves (Fig. 5c) indicate nonlinear current dependence based on the LTEM observation in Fig. 4. The in-plane magnetization change is complicated with changing ripples and vague V cores due to the strong electric current interaction with the magnetization while increasing the electric current. After stabilization by the strong stimulus of the electric current, the V nucleation and annihilation along the cross-tie DW become simple and clear as the reversed electric current increases from 0 to −1000 mA. The stabilized number of Vs remains almost the same with cross-tie DWs (Fig. 4i and l).

In our experiments, the periodic DW nucleation/annihilation and the displacement between different metastable states are dominant. The periodic V nucleation and annihilation due to the spin transfer torque were predicted by micromagnetic calculations above the breakpoint, whereas the spin transfer torque is balanced by an internal restoring torque at low current [40]. The different metastable magnetic states are separated by an effective energy barrier. A strong electric current, such as 1000 or −1000 mA for this sample, may drive to a metastable state with deep potential wells, and a large energy barrier separates it from other magnetic states. The electric current-driven DW motion and nucleation in our experiment indicates the effective interaction of the electric current on the magnetic V because of the high-spin momentum transfer efficiency [41].

### 3.3. Magnetic domain evolution under in-plane magnetic field

The DW motion behavior driven by in-plane magnetic fields is investigated by *in situ* LTEM at RT. The reversed magnetic field is applied to the remnant magnetic state after magnetic saturation at more than 400 Oe. The magnetization reversal of the amorphous Ce<sub>14</sub>Fe<sub>80</sub>B<sub>6</sub> ribbon is shown in Fig. 6. The magnetization remains uniform contrast until DWs occur at the reversed field of −0.3 Oe (Fig. 6a). V prefers to initiate nucleation from the edge under the magnetic field of −5.2 Oe (Fig. 6b). The DWs nucleate further as the field increases to −6.9 Oe (Fig. 6c), and the remarkable nucleation of Vs and AVs occur when the field increases to −10.0 Oe (Fig. 6d). Vs and AVs begin to annihilate with priority on account of magnetization distribution [42] with a further increase in the reversed magnetic field (Fig. 6e–i). The contrast of in-plane magnetization ripple changes with the magnetic field. The relative direction relationship between the magnetic field and the main DW affects the magnetic domain evolution. The V/AV moves and annihilates if the magnetic field direction is normal to the main DW called hard-axis direction and buckles with the main DW when the magnetic field is parallel to the wall [43,44]. In our experiment, a large component of magnetic field is perpendicular to the DWs of I and II, with a small component being parallel to the DWs. Thus, Vs/AVs annihilate into the main DWs I and II (Fig. 6e), and a large field is needed to shift the main domain wall [45]. When the reversed magnetic field increases further, the Vs/AVs disappear, the DWs move toward the sample edge, and the magnetization finally aligns

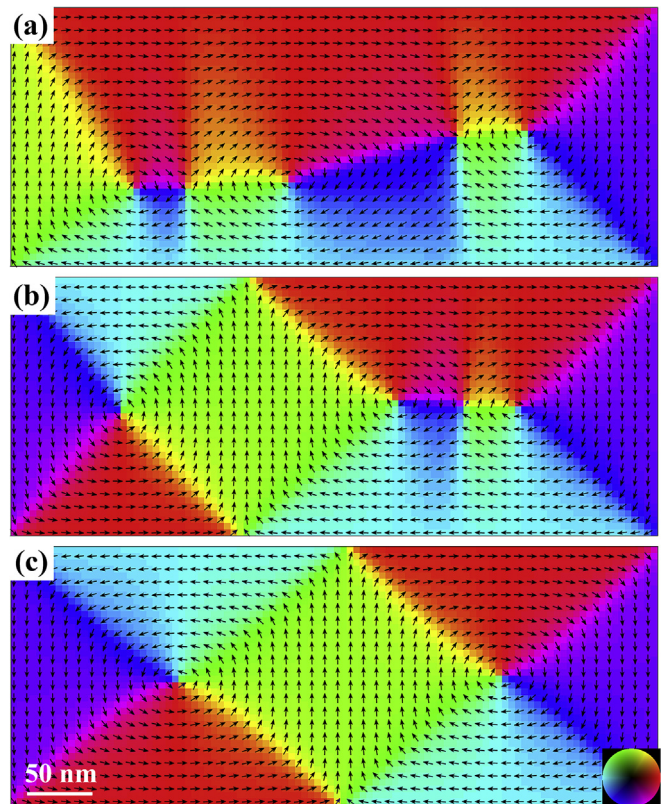


**Fig. 7.** Numerical micromagnetic simulations utilizing the OOMMF showing the magnetic domain configuration by altering the sample thickness. (a) Cross-tie domain wall with sample thickness  $t = 10$  nm. (b) Mixed state of vortex and cross-tie domain wall with sample thickness  $t = 20$  nm. (c) Vortex domain wall with sample thickness  $t = 100$  nm. The magnitude and orientation of the magnetization are depicted by the color and the arrows. (For interpretation of the references to colour in this figure legend, the reader is referred to the web version of this article).

parallel to the reversed field. Pinning effects due to different defects, such as edge and crack, are observed during the experiments.

### 3.4. Micromagnetic simulations

Numerical simulations based on the Landau–Lifshitz–Gilbert equation are performed with the use of the object-oriented micromagnetic framework (OOMMF). Results are shown in Fig. 7. The system consists of an amorphous Ce<sub>14</sub>Fe<sub>80</sub>B<sub>6</sub> strip with length  $l = 500$  nm, width  $h = 200$  nm, and variable thickness  $t$ . The typical material parameters of amorphous Ce<sub>14</sub>Fe<sub>80</sub>B<sub>6</sub>, i.e., saturation magnetization  $M_S = 930 \times 10^3$  Am<sup>−1</sup>, exchange constant  $A_{\text{ex}} = 4 \times 10^{-12}$  Jm<sup>−1</sup>, and the Gilbert damping constant  $\alpha = 0.5$ , are used. The cross-tie wall is the equilibrium DW structure for thin sample (Fig. 7a), and both cross-tie wall and V exist for medium thickness (Fig. 7b) with the isolated V forming in thick sample (Fig. 7c). This result confirms that the different initial magnetic domain configurations in conventionally made (Fig. 1) and FIB-made (Fig. 3) TEM samples are caused by the thickness differences.

## 4. Conclusions

In summary, the magnetic domain evolution of V, AV and cross-tie DWs under different external fields is clearly demonstrated in the amorphous Ce<sub>14</sub>Fe<sub>80</sub>B<sub>6</sub> ribbon via real-space LTEM imaging. The stabilized cross-tie DWs connected with V/AV pairs form at low temperature and after strong electric current stimulus. The V/AV

nucleation and annihilation in pairs with the complicated magnetization transformation caused by external stimulus, such as temperature, reversed magnetic field, and spin torque effect, are experimentally studied. The tunable nucleation and annihilation behavior under the external fields in amorphous Ce<sub>14</sub>Fe<sub>80</sub>B<sub>6</sub> ribbons without pattern constriction will provide a fruitful playground for fundamental physics and the exploration of the novel application of accumulated rare-earth resources.

## Acknowledgements

This work was supported by the National Basic Research Program of China (Grant No. 2014CB643702) and the National Key Research and Development Program of China (Grant No. 2016YFB0700902, 2016YFB0700903) and the National Natural Science Foundation of China (Grant No. 51590880, 11374349). The Knowledge Innovation Project of the Chinese Academy of Sciences (Grant No. KJZD-EW-M05) and the Youth Innovation Promotion Association, CAS, 2015004.

## References

- [1] S.S.P. Parkin, M. Hayashi, L. Thomas, Magnetic domain-wall racetrack memory, *Science* 320 (2008) 190–194.
- [2] D.A. Allwood, G. Xiong, C.C. Faulkner, D. Atkinson, D. Petit, R.P. Cowburn, Magnetic domain-wall logic, *Science* 309 (2005) 1688–1692.
- [3] M. Laufenberg, D. Backes, W. Bührer, D. Bedau, M. Kläui, U. Rüdiger, C.A.F. Vaz, J.A.C. Bland, L.J. Heyderman, F. Nolting, S. Cherifi, A. Locatelli, R. Belkhout, S. Heun, E. Bauer, Observation of thermally activated domain wall transformations, *Appl. Phys. Lett.* 88 (2006), 052507.
- [4] M. Klaui, P.O. Jubert, R. Allenspach, A. Bischof, J.A. Bland, G. Faini, U. Rudiger, C.A. Vaz, L. Vila, C. Vouille, Direct observation of domain-wall configurations transformed by spin currents, *Phys. Rev. Lett.* 95 (2005), 026601.
- [5] M. Eltschka, M. Wotzel, J. Rhensius, S. Krzyk, U. Nowak, M. Klaui, T. Kasama, R.E. Dunin-Borkowski, L.J. Heyderman, H.J. van Driel, R.A. Duine, Nonadiabatic spin torque investigated using thermally activated magnetic domain wall dynamics, *Phys. Rev. Lett.* 105 (2010), 056601.
- [6] S. Rößler, S. Hankemeier, B. Krüger, F. Balhorn, R. Frömter, H.P. Oepen, Nonadiabatic spin-transfer torque of magnetic vortex structures in a permalloy square, *Phys. Rev. B* 89 (2014), 174426.
- [7] N. Vernier, D.A. Allwood, D. Atkinson, M.D. Cooke, R.P. Cowburn, Domain wall propagation in magnetic nanowires by spin-polarized current injection, *Europhys. Lett.* 65 (2004) 526–532.
- [8] L. Thomas, R. Moriya, C. Rettner, S.S.P. Parkin, Dynamics of magnetic domain walls under their own inertia, *Science* 330 (2010) 1810–1813.
- [9] S.A. Montoya, S. Couture, J.J. Chess, J.C.T. Lee, N. Kent, D. Henze, S.K. Sinha, M.Y. Im, S.D. Kevan, P. Fischer, B.J. McMorrion, V. Lomakin, S. Roy, E.E. Fullerton, Tailoring magnetic energies to form dipole skyrmions and skyrmion lattices, *Phys. Rev. B* 95 (2017), 024415.
- [10] R. Hertel, C.M. Schneider, Exchange explosions: magnetization dynamics during vortex-antivortex annihilation, *Phys. Rev. Lett.* 97 (2006) 177202.
- [11] K.S. Lee, B.W. Kang, Y.S. Yu, S.K. Kim, Vortex–antivortex pair driven magnetization dynamics studied by micromagnetic simulations, *Appl. Phys. Lett.* 85 (2004) 1568–1570.
- [12] T. Okuno, K. Mibu, T. Shinjo, Two types of magnetic vortex cores in elliptical permalloy dots, *J. Appl. Phys.* 95 (2004) 3612–3617.
- [13] J.C. Slonczewski, Current-driven excitation of magnetic multilayers, *J. Magn. Magn. Mater.* 159 (1996) L1–L7.
- [14] G. Tatara, H. Kohno, Theory of current-driven domain wall motion: spin transfer versus momentum transfer, *Phys. Rev. Lett.* 92 (2004), 086601.
- [15] Z. Li, S. Zhang, Domain-wall dynamics driven by adiabatic spin-transfer torques, *Phys. Rev. B* 70 (2004), 024417.
- [16] A. Thiaville, Y. Nakatani, J. Miltat, N. Vernier, Domain wall motion by spin-polarized current: a micromagnetic study, *J. Appl. Phys.* 95 (2004) 7049–7051.
- [17] S. Zhang, Z. Li, Roles of nonequilibrium conduction electrons on the magnetization dynamics of ferromagnets, *Phys. Rev. Lett.* 93 (2004), 127204.
- [18] B.E. Argyle, E. Terenzio, J.C. Slonczewski, Magnetic vortex dynamics using the optical cotton-mouton effect, *Phys. Rev. Lett.* 53 (1984) 190–193.
- [19] A.R. Völkel, G.M. Wysin, F.G. Mertens, A.R. Bishop, H.J. Schnitzer, Collective-variable approach to the dynamics of nonlinear magnetic excitations with application to vortices, *Phys. Rev. B* 50 (1994) 12711–12720.
- [20] K.Y. Gusienko, B.A. Ivanov, V. Novosad, Y. Otani, H. Shima, K. Fukamichi, Eigenfrequencies of vortex state excitations in magnetic submicron-size disks, *J. Appl. Phys.* 91 (2002) 8037–8039.
- [21] J.P. Park, P. Eames, D.M. Engebretson, J. Berezovsky, P.A. Crowell, Imaging of spin dynamics in closure domain and vortex structures, *Phys. Rev. B* 67 (2003) 020403.
- [22] L. Berger, Exchange interaction between ferromagnetic domain wall and electric current in very thin metallic films, *J. Appl. Phys.* 55 (1984) 1954–1956.
- [23] V. Uhlíř, S. Pizzini, N. Rougemaille, V. Cros, E. Jiménez, L. Ranno, O. Fruchart, M. Urbánek, G. Gaudin, J. Camarero, C. Tiegs, F. Sirotti, E. Wagner, J. Vogel, Direct observation of Oersted-field-induced magnetization dynamics in magnetic nanostripes, *Phys. Rev. B* 83 (2011) 020406.
- [24] A. Thiaville, Y. Nakatani, J. Miltat, Y. Suzuki, Micromagnetic understanding of current-driven domain wall motion in patterned nanowires, *Europhys. Lett.* 69 (2005) 990–996.
- [25] M. Kläui, M. Laufenberg, L. Heyne, D. Backes, U. Rüdiger, C.A.F. Vaz, J.A.C. Bland, L.J. Heyderman, S. Cherifi, A. Locatelli, T.O. Mentes, L. Aballe, Current-induced vortex nucleation and annihilation in vortex domain walls, *Appl. Phys. Lett.* 88 (2006) 232507.
- [26] M. Zhang, Z.B. Li, B.G. Shen, F.X. Hu, J.R. Sun, Variations of phase constitution and magnetic properties with Ce content in Ce-Fe-B permanent magnets, *J. Alloys Compd.* 651 (2015) 144–148.
- [27] X. Wang, M. Zhu, W. Li, L. Zheng, D. Zhao, X. Du, A. Du, The microstructure and magnetic properties of melt-spun CeFeB ribbons with varying Ce content, *Mater. Lett.* 11 (2015) 109–112.
- [28] J.F. Herbst, M.S. Meyer, F.E. Pinkerton, Magnetic hardening of Ce<sub>2</sub>Fe<sub>14</sub>B, *J. Appl. Phys.* 111 (2012), 07A718.
- [29] Z.B. Li, L.L. Zhang, X.F. Zhang, Y.F. Li, Q. Zhao, T.Y. Zhao, B.G. Shen, Tunable Curie temperature around room temperature and magnetocaloric effect in ternary Ce–Fe–B amorphous ribbons, *J. Phys. D. Appl. Phys.* 50 (2017) 015002.
- [30] Z.B. Li, M. Zhang, B.G. Shen, F.X. Hu, J.R. Sun, Variations of phase constitution and magnetic properties with Ce content in Ce-Fe-B permanent magnets, *Mater. Lett.* 172 (2016) 102–104.
- [31] G. Mihajlović, M.S. Patrick, J.E. Pearson, V. Novosad, S.D. Bader, M. Field, G.J. Sullivan, A. Hoffmann, Temperature dependent nucleation and annihilation of individual magnetic vortices, *Appl. Phys. Lett.* 96 (2010) 112501.
- [32] C.Y. Yang, Y.H. Lu, W.H. Lin, M.H. Lee, Y.J. Hsu, Y.C. Tseng, Structural imperfections and attendant localized/itinerant ferromagnetism in ZnO nanoparticles, *J. Phys. D. Appl. Phys.* 47 (2014), 345003.
- [33] K.C. Verma, R.K. Kotnala, Understanding lattice defects to influence ferromagnetic order of ZnO nanoparticles by Ni, Cu, Ce ions, *J. Solid State Chem.* 246 (2017) 150–159.
- [34] S. Basu, D.Y. Inamdar, S. Mahamuni, A. Chakrabarti, C. Kamal, G.R. Kumar, S.N. Jha, D. Bhattacharyya, Local structure investigation of cobalt and manganese doped ZnO nanocrystals and its correlation with magnetic properties, *J. Phys. Chem. C* 118 (2014) 9154–9164.
- [35] J.K. Furdyna, N. Samarth, R.B. Frankel, J. Spalek, Static magnetic susceptibility of Zn<sub>1-x</sub>Mn<sub>x</sub>Se, *Phys. Rev. B* 37 (1988) 3707–3709.
- [36] E.M. Hempe, M. Kläui, T. Kasama, D. Backes, F. Junginger, S. Krzyk, L.J. Heyderman, R. Dunin-Borkowski, U. Rüdiger, Domain walls, domain wall transformations and structural changes in permalloy nanowires when subjected to current pulses, *Phys. Status Solidi (a)* 204 (2007) 3922–3928.
- [37] K.I. Metlov, Cross-tie domain wall ground state in thin films, *J. Low. Temp. Phys.* 139 (2005) 207–219.
- [38] W. Burger, Lorentz electron microscopic studies on cross-tie density and on formation and annihilation of Bloch line pairs in cross-tie walls, *Phys. Status Solidi 4* (1971) 723–730.
- [39] A.C.C. Yu, A. Petford-Long, T. Miyazaki, Direct observation of domain structure and magnetization reversal of magnetic thin films using Lorentz transmission electron microscopy, *J. Appl. Phys.* 40 (2001) 4891–4896.
- [40] V. Estévez, L. Laurson, Head-to-head domain wall structures in wide permalloy strips, *Phys. Rev. B* 91 (2015), 054407.
- [41] D. Ravelosona, D. Lacour, J.A. Katine, B.D. Terris, C. Chappert, Nanometer scale observation of high efficiency thermally assisted current-driven domain wall depinning, *Phys. Rev. Lett.* 95 (2005) 117203.
- [42] H.H. Liu, X.K. Duan, R.C. Che, Z.F. Wang, X.F. Duan, In situ Lorentz microscopy observation of displaced chain walls in permalloy, *Mater. Trans.* 50 (2009) 1660–1663.
- [43] W. Burger, Lorentz electron microscopic studies on migration of Bloch lines and buckling of cross-tie walls, *Phys. Status Solidi 4* (1971) 713.
- [44] E.J. Torok, D.S. Lo, H.N. Oredson, W.J. Simon, Magnetization creep of cross-tie walls, *J. Appl. Phys.* 40 (1969) 1222–1224.
- [45] R.V. Telesnin, E.N. Ilycheva, N.G. Kanavina, V.E. Osukhovskii, A.G. Shishkov, Creep kinematics of cross-tie domain walls, *Phys. Status Solidi 34* (1969) 443–449.